Ludwig–Soret effect formulated from the grain-boundary-phase model

*Toshiyuki Koyama[1)] and Yuhki Tsukada[1)]

[1)] Department of Materials Design Innovation Engineering,
Graduate School of Engineering, Nagoya University
Furo-cho, Chikusa-ku, Nagoya 464-8603, JAPAN
Phone/Fax: +81-52-789-3613, E-mail: koyama@material.nagoya-u.ac.jp
*Corresponding author

Keywords: thermal diffusion, Gibbs energy, vacancy, simulation, diffusion equation, flash sintering

Abstract

The Ludwig–Soret effect is a phenomenon wherein thermal diffusion is induced by a temperature gradient. The governing differential equation to explain this phenomenon has been derived phenomenologically based on the Onsager theorem in non-equilibrium thermodynamics. In this study, we applied the grain-boundary-phase (GBP) model to the Ludwig–Soret effect. This model has been originally proposed for calculating the amount of grain boundary segregation in alloys. The flux equation for the thermal diffusion of vacancies was reasonably derived through parallel-tangent construction of the Gibbs energy curves utilized in the GBP model. Moreover, the thermal vacancy diffusion in a pure metal was simulated. The results illustrated that the excess vacancies in the pure metal preferentially moved to the high-temperature region. The direct application of the thermodynamic Gibbs energy parameters in the CALPHAD method is essential to analyze the thermal diffusion phenomenon. Furthermore, the oxygen vacancy diffusion in $Zr(O,Va)_2$ under a considerably large temperature gradient was calculated, and a similar result was obtained, wherein the excess oxygen vacancies moved to the high-temperature region. This finding may explain the rapid atom diffusion observed during the flash sintering process.

1. Introduction

The Ludwig–Soret effect [1,2] is a phenomenon in materials wherein thermal diffusion is induced by a temperature gradient. The governing differential equation [1,2] to explain the Ludwig–Soret effect has been derived phenomenologically based on the Onsager theorem in non-equilibrium thermodynamics. This equation is shown as Eq. (1):

$$J = -D_c \nabla c - D_T c_0 (1 - c_0) \nabla T, \tag{1}$$

where c_0 is the average solute composition, and $c(\boldsymbol{r},t)$ is the local solute composition, which is a function of local position $\boldsymbol{r}$ ($\boldsymbol{r}$ = x, y, z) and time t. D_c and D_T are the diffusion coefficients for the solute diffusion induced by a composition gradient and a temperature gradient, respectively. As summarized in recent reviews on the Ludwig–Soret effect [3-5], Eq. (1) can be modified; however, the basic concept for deriving Eq. (1) from the Onsager theorem remains the same.

In this study, we applied the grain-boundary-phase (GBP) model [6-8] in deriving the equation for the thermal diffusion of vacancies. The thermal diffusion of vacancies in metals has been discussed by Shewmon [9,10] in terms of the Ludwig–Soret effect based on Eq. (1). Original GBP model has been proposed by Hillert [6,7] to calculate the amount of grain boundary segregation in alloys. In the GBP model, the parallel-tangent construction [6-8] to the Gibbs energy curves is a key technique for estimating the amount of grain boundary segregation. As explained in this article, the governing equation for the Ludwig–Soret effect, Eq. (1), was also derived based on the same technique of parallel-tangent construction to the Gibbs energy curves. Henceforth, the parallel-tangent construction to the Gibbs energy curves is referred simply as the "parallel-tangent method." This approach has several merits. The thermodynamic data of Gibbs energy are accumulated through the CALPHAD (Calculation of phase diagrams) method [11,12], and these thermodynamic data can be directly applied to analyze the dynamics of the Ludwig–Soret effect through the parallel-tangent method. We can use the quantitative data in the CALPHAD method; hence, the extreme phenomenon under a large temperature gradient will be satisfactorily clarified. This suggests that the thermodynamic data in the CALPHAD method open a new way to analyze the thermal diffusion phenomenon, that is, we can simultaneously calculate the atom diffusion induced by not only a composition field but also a temperature field.

In this paper, we first demonstrate the equivalency between the parallel-tangent method and the Ludwig–Soret effect theory. We then apply this approach to undertand the thermal diffusion behavior of vacancies in a pure metal and the thermal diffusion of oxygen vacancies in $Zr(O,Va)_2$. Furthermore, the mechanism of rapid atom diffusion, which was

recently observed experimentally during a flash sintering process [13-17], is discussed on the basis of the calculation results.

2. Parallel-tangent method and Ludwig–Soret effect

In this section, we explain the original GBP model and the relationship between the parallel-tangent method and the Ludwig–Soret effect.

2.1 GBP model

The GBP model was proposed by Hillert as a method for estimating the extent of grain boundary segregation [6-8], wherein the grain boundary region is regarded as a thin film of an amorphous phase. This amorphous phase is often denoted as a GBP; hence, this method is described in the GBP model. Grain boundary segregation is estimated by calculating the equilibrium composition in the GBP. When we consider an A–B binary alloy system, where the α matrix phase is a solid solution phase and the β phase denotes the GBP, the equilibrium solute composition in the β phase is the segregation composition that we want to determine. However, the volume fraction of the β phase (f_β) must be constant because we disregard the polycrystalline microstructur change of the α matrix phase. Hence, the solute composition in the β phase(c_β) is not a composition on the equilibrium phase diagram, but a restricted composition under the condition of a fixed volume fraction f_β . The value of c_β is calculated by the Lagrange multiplier method, and the Gibbs energy of the (α+β) two-phase mixture G_c is given by

$$G_c = G_c^\alpha(c_\alpha, T) f_\alpha + G_c^\beta(c_\beta, T) f_\beta + \lambda(c_0 - c_\alpha f_\alpha - c_\beta f_\beta),$$

where λ is a Lagrange multiplier [18]; c_α and c_β are the compositions of the α and β phases, respectively; and c_0 is the average composition. f_α ($f_\alpha = 1 - f_\beta$) is the volume fraction of the α phase. $G_c^\alpha(c_\alpha, T)$ and $G_c^\beta(c_\beta, T)$ are the Gibbs energies of the α and β phases, respectively. These Gibbs energies are functions of composition and temperature T. The minimum condition of G_c is calculated as follows:

$$\frac{\partial G_c}{\partial c_\alpha} = \left(\frac{\partial G_c^\alpha}{\partial c_\alpha} - \lambda \right) f_\alpha = 0, \qquad \frac{\partial G_c}{\partial c_\beta} = \left(\frac{\partial G_c^\beta}{\partial c_\beta} - \lambda \right) f_\beta = 0, \qquad \frac{\partial G_c}{\partial \lambda} = c_0 - (c_\alpha f_\alpha + c_\beta f_\beta) = 0.$$

Subsequently, we obtained the parallel-tangent method, that is, parallel-tangent

construction to the Gibbs energy curves:

$$\frac{\partial G_c^{\alpha}}{\partial c_{\alpha}} = \frac{\partial G_c^{\beta}}{\partial c_{\beta}}, \qquad c_{\alpha} f_{\alpha} + c_{\beta} f_{\beta} = c_0 .$$

Phase compositions c_{α} and c_{β}, which satisfy the above equations, are the equilibrium compositions under the constraint of fixed f_{β}. Figure 1 shows the comparison between the conventional common-tangent construction of the Gibbs energy curves and the parallel-tangent method. The conventional common-tangent construction [19] of the Gibbs energy curves is explained by the same formulation in Appendix A for reference.

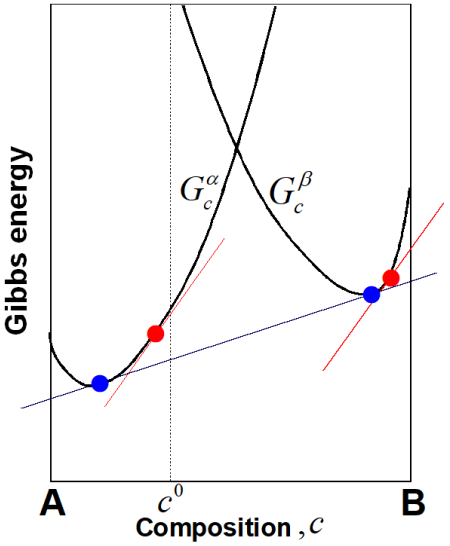

Fig. 1 Comparison between the conventional common-tangent construction of Gibbs energy curves and the parallel-tangent method.

2.2 Application of the GBP model in an inhomogeneous temperature field

Here, we consider that a single α phase and two regions with different temperatures T_1 and T_2 are in equilibrium, as shown in Fig. 2. The volume fractions of the regions denoted by T_1 and T_2 are f_1 and f_2, respectively. These regions are in contact with each other. The Gibbs energy of the system can be expressed as

$$G_c = G_c^{\alpha}(c_1, T_1) f_1 + G_c^{\alpha}(c_2, T_2) f_2 + \lambda_T (c_0 - c_1 f_1 - c_2 f_2) ,$$

where λ_T is the Lagrange multiplier. By calculating in the same way explained in the previous section, we obtain similar relations:

$$\frac{\partial G_c^{\alpha}(c_1, T_1)}{\partial c_1} = \frac{\partial G_c^{\alpha}(c_2, T_2)}{\partial c_2}, \quad c_1 f_1 + c_2 f_2 = c_0 .$$

Compositions c_1 and c_2, which satisfy the above equations, are the equilibrium compositions under the constraint of a fixed temperature field. Interestingly, this formulation is the same as the case of the

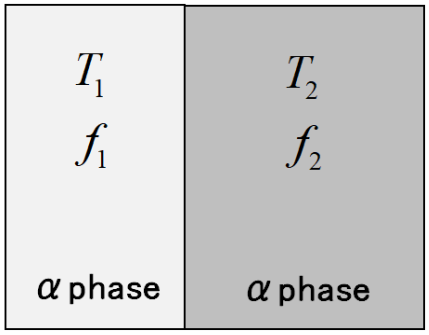

Fig. 2 Calculation conditions.

GBP model. In particular, the temperature field is unimportant in this case; however, this field plays a role in defining both the volume fractions of the two temperature regions and the two Gibbs energy curves ($G_\alpha(c_1,T_1)$ and $G_\alpha(c_2,T_2)$) at different temperatures.

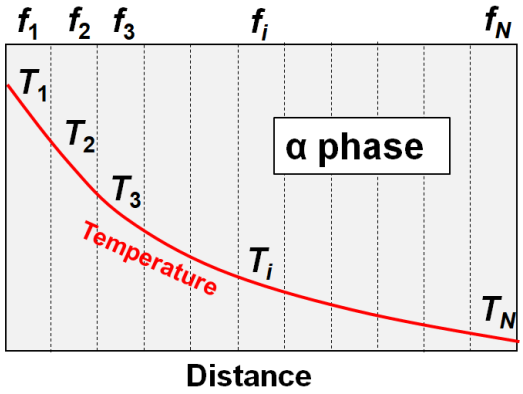

Fig. 3 Continuous temperature field.

Furthermore, if we consider a continuous temperature gradient, it can be approximated by many adjacent regions with different temperatures (Fig. 3), where N is the number of divisions. If N is large, the temperature of each divided region is assumed to be constant. The temperatures, volume fractions, and compositions in the divided individual regions are denoted by $T_i,(i=1,2,\cdots,N)$, $f_i,(i=1,2,\cdots,N)$, and $c_i,(i=1,2,\cdots,N)$, respectively. The Gibbs energy of the system can be expressed as

$$G_{\mathrm{c}}=\sum_{i=1}^{N} f_i G_\alpha(c_i,T_i)+\lambda_{\mathrm{T}}\left(c_0-\sum_{i=1}^{N} c_i f_i\right),$$

such that the minimizing Gibbs energy G_{c} provides

$$\frac{\partial G_{\mathrm{c}}}{\partial c_i}=\frac{\partial G_\alpha(c_i,T_i)}{\partial c_i} f_i-\lambda_{\mathrm{T}} f_i=0, \qquad \frac{\partial G_{\mathrm{c}}}{\partial \lambda_{\mathrm{T}}}=c_0-\sum_{i=1}^{N} c_i f_i=0.$$

Subsequently, the generalized parallel-tangent method is obtained.

$$\begin{aligned}&\frac{\partial G_\alpha(c_i,T_i)}{\partial c_i}=\frac{\partial G_\alpha(c_j,T_j)}{\partial c_j}, \quad (i,j=1,2,\cdots,N),\\ &\sum_{i=1}^{N} c_i f_i=c_0.\end{aligned} \tag{2}$$

Using these equations, we can calculate the equilibrium solute composition profile under a fixed continuous temperature gradient in this case. From the above discussion, the thermal diffusion flux of solute element J is expressed phenomenologically as follows:

$$J = -M_0 c(1-c)\nabla \frac{dG_\alpha}{dc} \tag{3}$$

where c is the local solute composition, and M_0 is the mobility of atom diffusion. If we perform the diffusion simulation using Eq. (3) under a fixed temperature field, we can determine the steady-state solute composition profile that satisfies Eq. (2).

3. Governing equation of the Ludwig–Soret effect

The governing equation of the Ludwig–Soret effect is derived from the GBP model. Here, we focused on vacancy diffusion in a pure metal under a temperature gradient for simplicity. The Gibbs energy is given by [19]

$$G = (H_\mathrm{F} - TS_\mathrm{F})c + RT\{(1-c)\ln(1-c) + c\ln c\}, \tag{4}$$

where c is the mole fraction of the vacancy, and R is the gas constant. H_F and S_F are the formation enthalpy and formation entropy of a vacancy, respectively. The equation for diffusion flux J of vacancies is obtained as follows:

$$\begin{aligned}
J &= -M_0 c(1-c)\nabla \frac{dG}{dc} = -M_0 c(1-c)\nabla\left[H_\mathrm{F} - TS_\mathrm{F} + RT\{\ln c - \ln(1-c)\}\right] \\
&= -M_0 c(1-c)\frac{\partial\left[H_\mathrm{F} - TS_\mathrm{F} + RT\{\ln c - \ln(1-c)\}\right]}{\partial c}\nabla c \\
&\quad - M_0 c(1-c)\frac{\partial\left[H_\mathrm{F} - TS_\mathrm{F} + RT\{\ln c - \ln(1-c)\}\right]}{\partial T}\nabla T \\
&= -M_0 c(1-c)\frac{RT}{c(1-c)}\nabla c - M_0 c(1-c)\left[-S_\mathrm{F} + R\{\ln c - \ln(1-c)\}\right]\nabla T \\
&= -M_0 RT\nabla c + M_0 \frac{H_\mathrm{F} - dG/dc}{T}c(1-c)\nabla T \\
&= -D_\mathrm{c}\nabla c + D_\mathrm{T} c(1-c)\nabla T,
\end{aligned} \tag{5}$$

where we defined $D_\mathrm{T} \equiv M_0(H_\mathrm{F} - dG/dc)/T$, and $D_\mathrm{c} \equiv M_0 RT$ is the Einstein equation [9]. Eq. (1), which is the governing equation of the Ludwig–Soret effect, is directly derived from the Gibbs energy function and the parallel-tangent method.

Recently, it has been discussed that how to treat the vacancy component in the compound energy formalism [20-23], and more accurate formula of the Gibbs energy function than

eq. (4) has been proposed. To evaluate the thermal vacancy composition quantitatively, it is necessary to use thermodynamic parameters and Gibbs energy functions optimized for vacancies as discussed in the papers [20-23]. Since the main objective of this study is to clarify the relationship between the thermal diffusion behavior and the Hillert's grain-boundary-phase model, we dared to use the Gibbs energy function of eq. (4) for the convenience to compare the previous studies by Shewmon [9,10].

4. Computer simulation on the thermal diffusion of vacancies

The steady-state vacancy composition profile in a pure metal under a temperature gradient was calculated. Figure 4 shows the condition of the temperature field used in the simulation. For simplicity, the temperature profile was assumed to be linear, and the profile shape was unchanged during the simulation of vacancy diffusion.

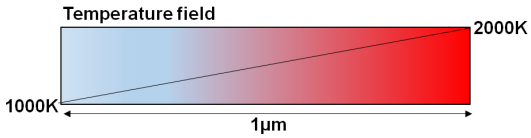

Fig. 4 Simulation condition with respect to the temperature field.

4.1 Local equilibrium composition of vacancies

The thermal equilibrium composition of vacancies at temperature T is given by Eq. (6):

$$c(T) = \exp\left(\frac{S_F}{R}\right)\exp\left(-\frac{H_F}{RT}\right) \tag{6}$$

Figure 5 shows the composition profile of vacancies calculated according to the local temperature using Eq. (6), where we assumed $H_F = 1.6\,(\mathrm{eV})$ and $S_F = R$. The vacancy composition increased with increasing temperature. Furthermore, the average composition

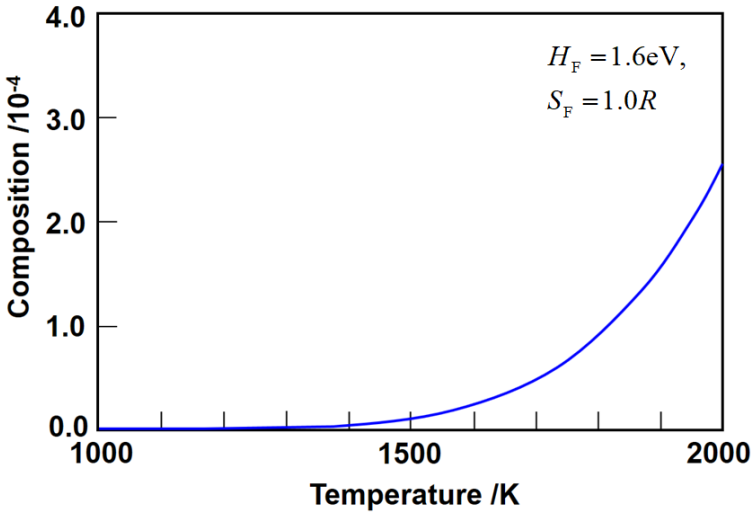

Fig. 5 Thermal equilibrium composition profile of vacancies determined from the local temperature.

of vacancies in the entire region in Fig. 4 was calculated as $c_0 = 4.6\times10^{-5}$.

4.2 Calculation of vacancy composition profile using the thermal diffusion equation

According to Eq. (3), the equation for the thermal diffusion of vacancies is derived as follows:

$$\begin{aligned} \frac{dc}{dt} &= \nabla\cdot\left\{M_0 c(1-c)\nabla\frac{dG}{dc}\right\} \cong M_0 c_0(1-c_0)\nabla^2\frac{dG}{dc}, \\ \frac{dG}{dc} &= H_F - TS_F + RT\left\{\ln c - \ln(1-c)\right\} \end{aligned} \tag{7}$$

Here, we focused on the steady-state vacancy composition profile, which is determined by a long-term simulation. Hence, we assumed that $M_0 c(1-c) = M_0 c_0(1-c_0)$ and $M_0 = 1$. The numerical simulation method to calculate the steady-state vacancy composition profile is a conventional finite difference method [24], where the one-dimensional space of Fig. 4 was divided into 100. The temporal change of the composition profile was simulated by the Euler method, and the calculation was finished when the composition profile was no longer changed. The detail of the simulation method is available in ref [24].

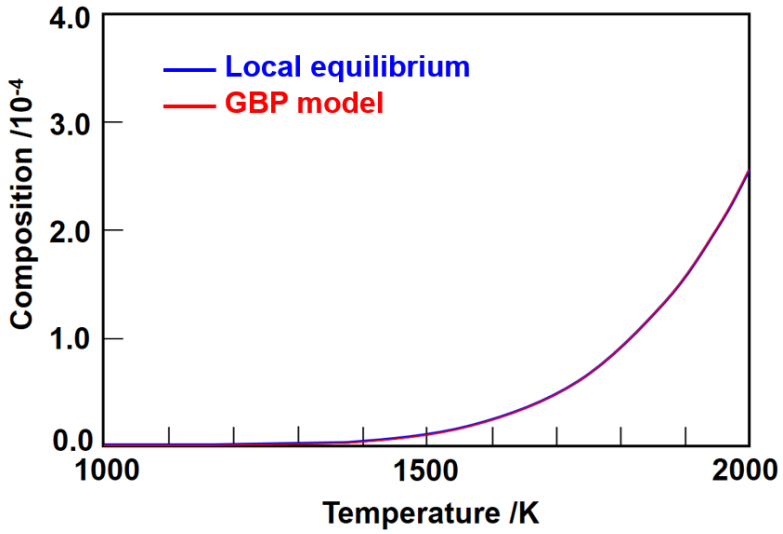

Fig. 6 Thermal equilibrium composition profile of vacancies calculated from the thermal diffusion equation.

Fig. 6 shows the steady-state composition profile of vacancies calculated using Eq. (7). In this profile, the average composition c_0 of the vacancies was set to 4.6×10^{-5}, which is the same as that from Fig. 5. The calculated steady-state composition profile (red curve in

Fig. 6) coincided completely with that shown in Fig. 5 (blue curve in Fig. 6). This result is because the parallel-tangent construction in Eq. (2) calculates the local equilibrium state, where the slope of the parallel-tangent line is zero.

In contrast, if we assumed an excess vacancy composition, where $c_0 = 7.0\times10^{-5}$, the calculated steady-state composition profile of vacancies was illustrated as the red curve in Fig. 7. The blue curve is the same as that shown in Fig. 6. Interestingly, the vacancy composition preferentially increased in the high-temperature region. The purpose of this calculation is to understand which direction the vacancies will move according to the thermal diffusion if there are excess vacancies. Therefore, the excess vacancies were introduced and the vacancy composition was assumed to be a conserved quantity to confirm the flow of vacancies.

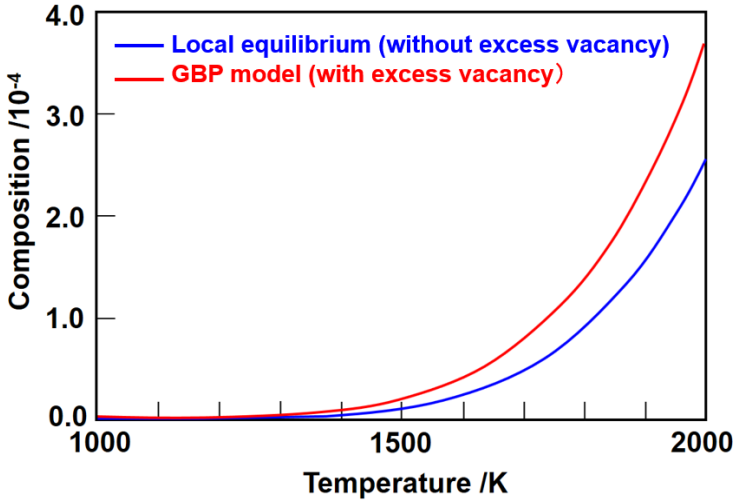

Fig. 7 Thermal equilibrium composition profile of vacancies calculated from the thermal diffusion equation with excess vacancy concentration.

When excess vacancies were introduced, the vacancies moved to the high-temperature region. This behavior is theoretically explained as follows:

At different temperatures T_1 and T_2, the Gibbs energy curves are approximated as follows:

$$G(T_1) = A(T_1) + \frac{1}{2}B(T_1)(c - c_{01})^2,$$
$$G(T_2) = A(T_2) + \frac{1}{2}B(T_2)(c - c_{02})^2. \qquad (8)$$

This approximation was performed around c_{0i} (i= 1, 2), which are the equilibrium vacancy compositions at temperature T_i. $A(T_i)$ and $B(T_i)$ are functions of T_i. Fig. 8 shows a schematic of the Gibbs energy curves according to Eq. (8). We assumed $T_1 < T_2$; hence, the relationships $A(T_1) > A(T_2)$ and $B(T_1) > B(T_2)$ should be satisfied because of the entropy effect in the Gibbs energy. The red lines in Fig. 8 are an example of the parallel-tangent method; c_1 and c_2 are the vacancy compositions at tangent points. Substituting Eq. (8) in Eq. (2), we obtain the following relation:

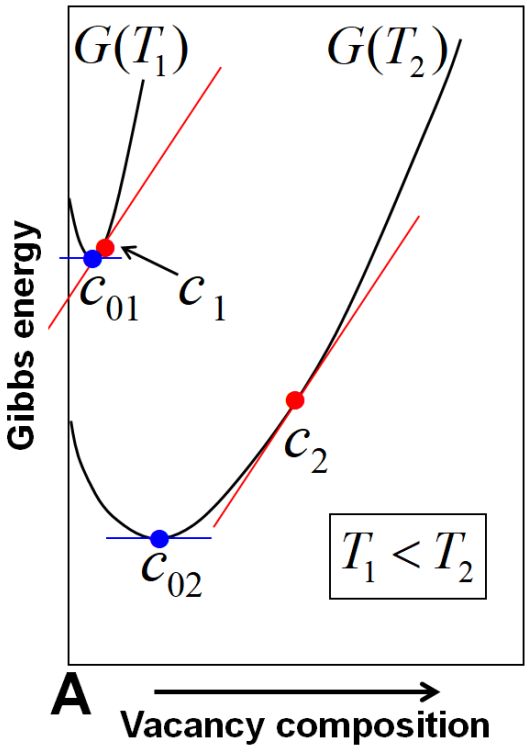

Fig. 8 Calculation condition.

$$B(T_1)(c_1 - c_{01}) = B(T_2)(c_2 - c_{02}), \qquad \therefore \frac{B(T_1)}{B(T_2)} = \frac{c_2 - c_{02}}{c_1 - c_{01}},$$

where compositions c_1 and c_2 are determined from the above equation. Also, $B(T_1) > B(T_2)$. Hence, the logic below can be easily understood.

$$\frac{B(T_1)}{B(T_2)} = \frac{c_2 - c_{02}}{c_1 - c_{01}} > 1, \qquad \therefore\ c_2 - c_{02} > c_1 - c_{01}$$

Therefore, the composition deviation ($c_i - c_{0i}$) from the thermal equilibrium composition increases with increasing temperature. This result corresponds to the simulation result in Fig. 7. In contrast, Shewmon insisted on the opposite conclusion that the vacancies move from the high-temperature to low-temperature region. This discrepancy is discussed in Appendix B.

5. Application to flash sintering

In this section, we discuss the rapid atom diffusion observed during a flash sintering

process on the basis of the steady-state composition profile of oxygen ion vacancies under a constant temperature gradient in ZrO_2. The Gibbs energy of cubic $Zr(O,Va)_2$ [25] is given by Eq. (9):

$$G = \frac{1}{1+2y_{O^{2-}}^{II}}\left[\begin{array}{l} y_{O^{2-}}^{II}\,{}^{0}G_{Zr:O}^{\gamma ZrO_2} + y_{Va}^{II}\,{}^{0}G_{Zr:Va}^{\gamma ZrO_2} + y_{O^{2-}}^{II}y_{Va}^{II}\left({}^{0}L_{Zr:O,Va}^{\gamma ZrO_2} + {}^{1}L_{Zr:O,Va}^{\gamma ZrO_2}(y_{O^{2-}}^{II} - y_{Va}^{II})\right) \\ +4RT\left(y_{O^{2-}}^{II}\ln y_{O^{2-}}^{II} + y_{Va}^{II}\ln y_{Va}^{II}\right) \end{array}\right], \quad (9)$$

where $y_{O^{2-}}^{II}$ and y_{Va}^{II} are the sub-lattice compositions of oxygen atoms and oxygen vacancies in an anion lattice site (denoted as a sub-lattice II) in $Zr(O,Va)_2$, respectively. ${}^{0}G_{Zr:X}^{\gamma ZrO_2}$ is the Gibbs energy of ZrX_2 (X= O or Va), and ${}^{i}L_{Zr:O,Va}^{\gamma ZrO_2}\ (i=0,1)$ are the coefficients of the Redlich–Kister expansion [11,12]. These quantities were assessed by Liang *et al.* [25] as functions of temperature in the CALPHAD approach. The assessment is as follows [25]:

$$\begin{aligned} &{}^{0}G_{Zr:O}^{\gamma ZrO_2} - {}^{0}G_{Zr}^{hcp} - {}^{0}G_{O_2}^{gas} = -1014781.7 - 269.4T + 59.015088T\ln T - 17.726352T^2, \\ &{}^{0}G_{Zr:Va}^{\gamma ZrO_2} - {}^{0}G_{Zr}^{hcp} = 7600 - 0.9T, \\ &{}^{0}L_{Zr:O,Va}^{\gamma ZrO_2} = 295349.19 - 97.99689T, \quad {}^{1}L_{Zr:O,Va}^{\gamma ZrO_2} = -352804.04 + 117.88667T. \quad \text{(J/mol)} \end{aligned}$$

${}^{0}G_{O_2}^{gas}$ and ${}^{0}G_{Zr}^{hcp}$ are the Gibbs energies of the oxygen molecule and pure Zr of hexagonal crystal structure, respectively. The diffusion flux of oxygen vacancies is expressed as follows:

$$J = -M_0 y_{Va}^{II}(1 - y_{Va}^{II})\nabla\frac{dG}{dy_{Va}^{II}}.$$

Hence, the diffusion equation with respect to the composition of oxygen vacancies is approximated as

$$\frac{dy_{Va}^{II}}{dt} \cong M_0 y_{Va0}^{II}(1 - y_{Va0}^{II})\nabla^2\frac{dG}{dy_{Va}^{II}}.$$

M_0 is the mobility of oxygen vacancy diffusion. In the calculation, we assumed $M_0 = 1$ because we focused on the steady-state oxygen vacancy composition profile, which is

determined by long-term simulation. The temperature field in Fig. 4 is employed as the boundary condition to calculate the steady-state composition profile of oxygen vacancies.

Figure 9 shows the calculation result, where the blue curve is the case of the average oxygen vacancy composition, in this case, $y_0 = 1.79 \times 10^{-4}$. This value was calculated from the local equilibrium composition of oxygen vacancies at the local temperature. The red curve is the case where we considered excess oxygen vacancies. In this case, the average oxygen vacancy composition was assumed to be $y_0 = 1.0 \times 10^{-3}$. Similar to the case shown in Fig. 7, the oxygen vacancy composition increased with increasing temperature. In particular, the excess oxygen vacancies concentrated in the high-temperature region by thermal diffusion. It has been realized experimentally that the reduction reaction of oxygen atoms takes place by the local electric current or potential during the flush sintering, then additional excess oxygen vacancies are introduced and which promotes the kinetics of sintering [13,17]. In this study, as we want to understand which direction the vacancies will move according to the thermal diffusion if there are excess oxygen vacancies, we introduced the excess vacancies, and the vacancy composition was treated as a conserved quantity to confirm the flow of vacancies.

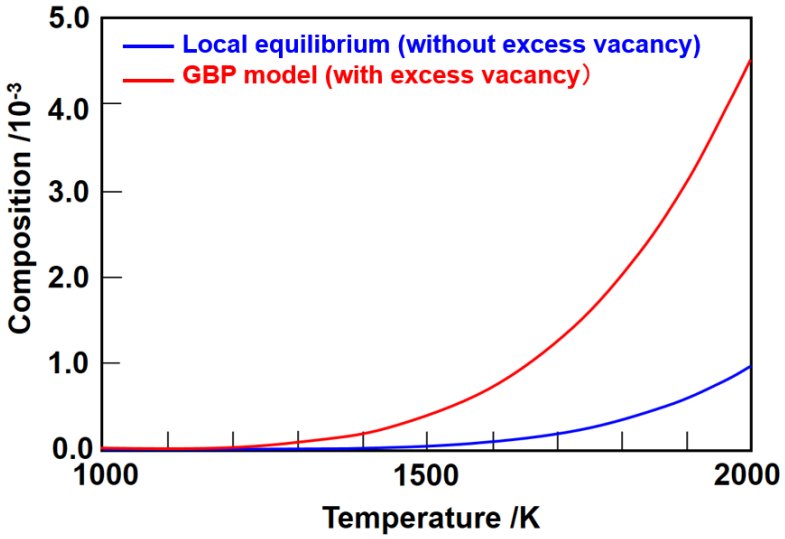

Fig. 9 Thermal equilibrium composition of oxygen vacancies calculated from the thermal diffusion equation.

Fig. 10 shows the schematic of the temperature field of the ZrO_2 particles during flash sintering [13,17]. The maximum temperature 2000 K in Fig. 10 was selected by considering the previous researches summarized in Ref. 13, and we assumed the furnace temperature, that is around 1000 K, as the minimum temperature in Fig. 10. Although the minimum temperature may be too low, we selected this temperature range for simplicity, because the following result of our proposal is not influenced.

In the flash sintering experiment, YSZ (Y_2O_3-stabilized ZrO_2) was often utilized [13-17],

and YSZ has many structural oxygen vacancies [26]. Flash sintering is one of the field-assisted sintering methods, and the electric current induces a large Joule heat. This heat enabled us to establish rapid sintering at low temperatures [15]. However, the mechanism of such rapid sintering at low temperatures is unclear because this phenomenon is insufficiently explained on the basis of Joule heat alone [16]. Furthermore, defect formation by oxide reduction during flash sintering is discussed as a trigger for the rapid sintering behavior [17].

The following explanation is only a speculation. However, we believe that the mechanism of flash sintering can be understood. The Joule heat at the surface region of the ZrO_2 particle provides a large temperature gradient, and Y addition introduces many excess oxygen vacancies (structural vacancies). Under such circumstances, the oxygen vacancy moves to the surface region from the inner side of the sintering particles according to the mechanism illustrated in Fig. 9. The vacancies promote the expansion of the crystal lattice [27], resulting in lattice softening, and Dong *et al.* has recently proposed that the introduction of oxygen ion vacancies would promote the diffusion of cations [28]. Hence, the cation atom diffusion at the surface region is extremely enhanced, and then the rapid diffusion of atoms is established in flash sintering.

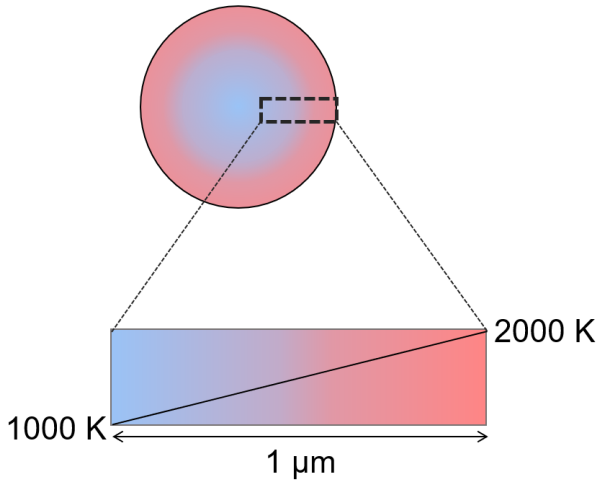

Fig.10 The schematic of the temperature field of the ZrO_2 particle during flush sintering.

6. Conclusions

In this study, the GBP model was applied to derive the flux equation of the Ludwig–Soret effect, and the thermal diffusion of vacancies was simulated. Furthermore, the proposed method was applied to explain the rapid atom diffusion observed during the flash sintering process. The results obtained are as follows:

(1) The flux equation of thermal diffusion by the Ludwig–Soret effect was reasonably derived through the parallel-tangent method utilized in the GBP model. Therefore, the thermodynamic Gibbs energy parameters in the CALPHAD method can be directly applied

to investigate the thermal diffusion phenomenon.

(2) The numerical simulation of thermal diffusion demonstrated that the excess vacancies in a pure metal move to the high-temperature region.

(3) Based on the proposed method, the oxygen vacancy diffusion in $Zr(O,Va)_2$ under a temperature gradient was calculated. The result obtained herein showed that the excess oxygen vacancies move to the high-temperature region. The localization of the oxygen vacancies in the high-temperature region may promote the rapid atom diffusion observed in YSZ during flash sintering in YSZ.

Acknowledgements

This work was supported by the Adaptable and Seamless Technology transfer Program (A-STEP), Japan Science and Technology Agency. Part of the present study was also supported by Grant-in-Aids for Scientific Research on Innovative Areas on High Entropy Alloys (the grant number JP18H05454) from the Ministry of Education, Culture, Sports, Science and Technology (MEXT) of Japan.

References

[1] S.R. de Groot, P. Mazur, Non-equilibrium Thermodynamics, Dover Publication Inc., New York, 1953.

[2] A. Katchalsky, P. F. Curran, Nonequilibrium Thermodynamics in Biophysics, Harvard Books in Biophysics, 2014.

[3] M. A. Rahman, M. Z. Saghir, Thermodiffusion or Soret effect: Historical review, Int. J. Heat and Mass Transfer, 73 (2014), 693–705. https://doi.org/10.1016/j.ijheatmasstransfer.2014.02.057.

[4] P. Costesèque, A. Mojtabi, J. K. Platten, Thermodiffusion phenomena, Comptes Rendus Mecanique, 339 (2011), 275–279. https://doi.org/10.1016/j.crme.2011.03.001.

[5] R. J. Asaro, D. Farkas, Y. Kulkarni, The Soret effect in diffusion in crystals, Acta Materialia, 56 (2008) 1243–1256. https://doi.org/10.1016/j.actamat.2007.11.019.

[6] M. Hillert, Phase Equilibria, Phase Diagrams and Phase Transformations: Their Thermodynamic Basis, Cambridge University Press, 2007.

[7] M. Hillert, Applications of Gibbs energy–composition diagrams, in: H. I. Aaronson (Ed.), Lectures on the theory of phase transformations, 2nd ed., TMS, Warrendale, PA, 1999, pp. 1–33.

[8] T. Nishizawa, Thermodynamics of Microstructures, ASM International, 2008.

[9] P. Shewmon, Diffusion in Solids, Wiley-TMS, 1991.

[10] P. Shewmon, Thermal Diffusion of Vacancies in Zinc, J Chem. Phys., 29 (1958) 1032–1036. https://doi.org/10.1063/1.1744650.

[11] N. Saunders, A. P. Miodownik, CALPHAD (Calculation of Phase Diagrams): A

Comprehensive Guide, Pergamon Press, 2014.
[12] H. Lukas, S. G. Fries, B. Sundman, Computational Thermodynamics: The Calphad Method, Cambridge University Press, 2007.
[13] M. Yu, S. Grasso, R. Mckinnon, T. Saunders and M. J. Reece, Review of flash sintering: materials, mechanisms and modelling, Advances in Applied Ceramics, 116 (2017) 24–60. https://doi.org/10.1080/17436753.2016.1251051.
[14] M. Cologna, B. Rashkova, R. Raj, Flash Sintering of Nanograin Zirconia in <5 s at 850°C, J. Am. Ceram. Soc., 93 (2010) 3556–3559. https://doi.org/10.1111/j.1551-2916.2010.04089.x.
[15] R. I. Todd, E. Zapata-Solvas, R. S. Bonilla, T. Sneddon and P.R. Wilshaw, Electrical characteristics of flash sintering: thermal runaway of Joule heating, J. Eur. Ceram. Soc., 35 (2015) 1865–1877. https://doi.org/10.1016/j.jeurceramsoc.2014.12.022.
[16] R. Raj, Analysis of the Power Density at the Onset of Flash Sintering, J. Am. Ceram. Soc., 99(2016) 3226–3232. https://doi.org/10.1111/jace.1417.
[17] T. Yamamoto, H. Yoshida, Flash Sintering of Oxide Ceramics and the Future Developments, materia Japan, 57 (2018) 373-380. https://doi.org/10.2320/materia.57.373.
[18] G. A. Korn, T. M. Korn, Mathematical Handbook for Scientists and Engineers: Definitions, Theorems, and Formulas for Reference and Review, Dover Pub., 2013. Lagrange multiplier method
[19] D. A. Porter, K. E. Easterling, M. Sherif, Phase Transformations in Metals and Alloys (Third Edition), CRC Press, 2009.
[20] P. Franke, Modeling of Thermal Vacancies in Metals within the Framework of the Compound Energy Formalism, J. Phase Equilb. Diffus., 35 (2014) 780-787. https://link.springer.com/article/10.1007/s11669-014-0348-0
[21] P.-W. Guan, Z.-K. Liu, A physical model of thermal vacancies within the CALPHAD approach, Scripta Mater., 133 (2017) 5-8.https://doi.org/10.1016/j.scriptamat.2017.02.002.
[22] T. Abe, K. Hashimoto, M. Shimono, C. Kocer, A description of vacancy complexes in an FCC solid solution within the framework of the CALPHAD Method, Calpahd, 63 (2018) 100-106. https://doi.org/10.1016/j.calphad.2018.08.010.
[23] J. Ågren, M. Hillert, Thermodynamic modelling of vacancies as a constituent, Calphad,13 (2019) 101666. https://doi.org/10.1016/j.calphad.2019.101666.
[24] W. H. Press, B. P. Flannery, S. A. Teukolsky, W. T. Vetterling, Numerical Recipes in C: The Art of Scientific Computing (2nd Ed.), Cambridge University Press, (1992).
[25] P.Liang, N.Dupin, S.G.Fries, H.J.Seifert, I.Ansara, H.L.Lukas, F.Aldinger, Thermodynamic assessment of the Zr-O binary system, Z. Metallkd, 92(2001) 747–756.
[26] Y.-M. Chiang, D. Birnie III, W. D. Kingery, Physical Ceramics: Principles for Ceramic Science and Engineering, John Wiley & Son, 1996. YSZ
[27] K. Amezawa, T. Kushi, K. Sato, A. Unemoto, S. Hashimoto, T. Kawada, Elastic moduli of $Ce_{0.9}Gd_{0.1}O_{2-\delta}$ at high temperatures under controlled atmospheres, Solid State Ionics 198 (2011) 32–38. https://doi.org/10.1016/j.ssi.2011.07.009.

[28] Y. Dong, H. Wang, I-W. Chen, Electrical and hydrogen reduction enhances kinetics in doped zirconia and ceria: I. grain growth study, J. Am. Ceram. Soc., 100 (2017) 876–886. https://doi.org/10.1016/j.ssi.2011.07.009. https://doi.org/10.1111/jace.14615.

Appendix A

Compared with the parallel-tangent method discussed in this study, the common-tangent construction [6-8,19] of the Gibbs energy curves is derived for reference. In equilibrium phase diagrams, the volume fractions of the constituent phases are functions of phase compositions c_α and c_β. Gibbs energy with the Lagrange multiplier term is expressed as

$$G_c = G_\alpha(c_\alpha,T)f_\alpha(c_\alpha,c_\beta) + G_\beta(c_\beta,T)f_\beta(c_\alpha,c_\beta) + \lambda[c_0 - c_\alpha f_\alpha(c_\alpha,c_\beta) - c_\beta f_\beta(c_\alpha,c_\beta)].$$

The minimization of Gibbs energy G_c is calculated by the following equations:

$$\frac{\partial G_c}{\partial c_\alpha} = \frac{\partial G_\alpha}{\partial c_\alpha} f_\alpha + G_\alpha \frac{\partial f_\alpha}{\partial c_\alpha} + G_\beta \frac{\partial f_\beta}{\partial c_\alpha} - \lambda\left(f_\alpha + c_\alpha \frac{\partial f_\alpha}{\partial c_\alpha} + c_\beta \frac{\partial f_\beta}{\partial c_\alpha} \right) = 0,$$

$$\frac{\partial G_c}{\partial c_\beta} = \frac{\partial G_\beta}{\partial c_\beta} f_\beta + G_\beta \frac{\partial f_\beta}{\partial c_\beta} + G_\alpha \frac{\partial f_\alpha}{\partial c_\beta} - \lambda\left(f_\beta + c_\beta \frac{\partial f_\beta}{\partial c_\beta} + c_\alpha \frac{\partial f_\alpha}{\partial c_\beta} \right) = 0,$$

$$\frac{\partial G_c}{\partial \lambda} = c_0 - c_\alpha f_\alpha - c_\beta f_\beta = 0.$$

From these equations, we obtained

$$\left(\frac{\partial G_\alpha}{\partial c_\alpha} - \lambda \right) f_\alpha + \{G_\beta - G_\alpha - \lambda(c_\beta - c_\alpha)\} \frac{\partial f_\beta}{\partial c_\alpha} = 0,$$

$$\left(\frac{\partial G_\beta}{\partial c_\beta} - \lambda \right) f_\beta + \{G_\beta - G_\alpha - \lambda(c_\beta - c_\alpha)\} \frac{\partial f_\beta}{\partial c_\beta} = 0.$$

The above two equations are identical equations. Hence, the following relations with respect to the common-tangent construction of the Gibbs energy curves are obtained:

$$\frac{\partial G_\alpha}{\partial c_\alpha} - \lambda = 0, \quad G_\beta - G_\alpha - \lambda(c_\beta - c_\alpha) = 0, \quad \frac{\partial G_\beta}{\partial c_\beta} - \lambda = 0,$$

$$\therefore \ \lambda = \frac{\partial G_\alpha}{\partial c_\alpha} = \frac{\partial G_\beta}{\partial c_\beta} = \frac{G_\beta - G_\alpha}{c_\beta - c_\alpha}, \quad (c_\alpha f_\alpha + c_\beta f_\beta = c_0).$$

Appendix B

According to the analysis of the thermal diffusion of vacancies by Shewmon [9,10], the

equation of the one-dimensional (x-direction) vacancy flux is as follows:

$$J_v = -L_{vv}\left[RT\left(\frac{\partial \ln c_v}{\partial c_v} \right)_T \frac{dc_v}{dx} + \left(\frac{Q_v^* - Q_1^*}{T} \right) \frac{\partial T}{\partial x} \right].$$

Q_v^* and Q_1^* are the heat of transport of the vacancies and atoms, respectively. c_v and T are the local vacancy composition and local temperature, respectively; these variables are functions of local position x and time t. L_{vv} is the mobility of vacancy diffusion, and R is the gas constant. $\{(Q_v^* - Q_1^*)/T\}(\partial T/\partial x)$ can take both positive and negative values; and, $RT\left(\partial \ln c_v / \partial c_v\right)_T \left(\partial c_v / \partial x\right)_T$ mainly determines the direction of vacancy diffusion. As Shewmon assumed the thermal equilibrium composition of vacancies that is determined from the local temperature, it can be considered that the higher the temperature is, the higher the vacancy composition will be. Thus, normal downhill diffusion takes place according to $RT\left(\partial \ln c_v / \partial c_v\right)_T \left(\partial c_v / \partial x\right)_T$, indicating that the vacancies move from the high-temperature to low-temperature region.

This argument is oversimplified because each point in the profile satisfies the thermal equilibrium composition, i.e., the vacancy composition profile is in a steady state with minimum Gibbs energy, then, no vacancy diffusion occurs (see Fig. 6). Therefore, the excess vacancies must be required to discuss the thermal diffusion of vacancies, as explained in this study.